Engineering Structures 59 (2014) 574–586

Contents lists available at ScienceDirect

Engineering Structures

journal homepage: www.elsevier.com/locate/engstruct

Elevated temperature resistance of welded tubular joints under axial load in the brace member

E. Ozyurt [a], Y.C. Wang [a,*], K.H. Tan [b]

[a] School of Mechanical, Aerospace and Civil Engineering, University of Manchester, UK
[b] Department of Civil and Environmental Engineering, Nanyang Technological University, Singapore

ARTICLE INFO

Article history:
Received 9 August 2013
Revised 7 November 2013
Accepted 11 November 2013

Keywords:
Circular hollow section (CHS)
Square hollow section (SHS)
T-joints
K-joints
X-joints
Y-joints
N-joints
Finite element model
Ultimate capacity
Elevated temperatures

ABSTRACT

This paper presents the results of a study to obtain the ultimate capacity of welded steel tubular joints at elevated temperatures. Finite Element (FE) simulations of welded tubular joints with axially loaded brace member made of CHS or SHS at different elevated temperatures were carried out using the commercial Finite Element software ABAQUS v6.10-1 [1]. After validation, extensive numerical simulations were conducted on T-, Y-, X-, N- and non-overlapped K-joints subjected to brace axial compression or tension, considering a wide range of geometrical parameters. The material and geometrical nonlinearities, which have significant influence on the ultimate strength of tubular joints at elevated temperatures, were taken into account. Uniform temperature distribution was assumed for both the chord and brace members.

Results of the numerical simulation were compared with calculation results using the design equations in Eurocode EN 1993-1-2 [3] and CIDECT design guide [16] but replacing the yield stress of steel at ambient temperature by those at elevated temperatures. It is found that for gap K- and N-joints and for T-, Y- and X-joints with the brace member under axial tensile load, this approach is suitable. However, for CHS T-, Y- and X-joints under brace compression load, this method overestimates the ultimate load carrying capacity of the joint. In fact, for these situations, the joint strength reduction at increasing temperatures follows more closely the reduction in the elastic modulus of steel at elevated temperatures.

1. Introduction

The popularity of hollow structural sections of all types has increased in the recent decades owing to their attractive appearance, light weight and structural advantages. They have been widely used in onshore and offshore structures e.g. bridges, towers, space-trusses, lattice girders, space-frame roof systems, offshore platforms, etc. For these structures, fire presents one of the most severe design conditions, because the mechanical properties of the steel degrade as the temperature increases. It is important that the behaviour of the tubular structures at high temperatures is thoroughly understood and reliable methods are available to calculate their strengths.

This paper investigates the behaviour of welded tubular structural joints at elevated temperatures. The ambient temperature behaviour of welded tubular joints has been subject to extensive research studies [17–21]. However, there is a paucity of research of their behaviour at elevated temperatures. Nguyen et al. [12,13] carried out both experimental and numerical analysis on the behaviour of welded tubular joints at elevated temperatures. In this research, they conducted five full scale circular hollow section (CHS) T-joints subjected to axial compression in the brace member at different temperatures. The results show that design guide predictions overestimated the ultimate load carrying capacity of axially loaded CHS T-joints at elevated temperatures. Cheng et al. [5] carried out some experimental tests and parametric simulations of CHS T-joints at elevated temperatures with the brace member in compression. They observed that the critical mode of joint failure was plastification of the chord face. They performed a number of numerical simulations to investigate the effects of different design parameters. However, they did not give any guidance on joint strength design calculation. He et al. [7] tested two tubular gap K-joints in order to investigate joint temperature development and structural behaviour under heating. They made a comparison between the joint failure loads from their tests and from their calculations using EN 1993-1-8 [4] with the elevated temperature steel strength. This comparison showed that the EN 1993-1-8 calculation result was safe in one case (test result higher than the calculation result by 17%) and unsafe (−7%) in the other case. However, a detailed examination of their definition of the joint failure temperature, based on an arbitrary rate of displacement, may be too conservative. Meng et al. [11] and Liu et al. [9] present some experimental and numerical research results of the structural behaviour of steel planar tubular trusses subjected to fire, although these publications do not address the issue of joint behaviour.

* Corresponding author.
E-mail address: yong.wang@manchester.ac.uk (Y.C. Wang).

0141-0296/$ - see front matter © 2013 Elsevier Ltd. All rights reserved.
http://dx.doi.org/10.1016/j.engstruct.2013.11.014

Nomenclature

CHS	circular hollow sections	L	length of chord
SHS	square hollow sections	l	length of brace
D	diameter of chord	P_{20}	ultimate joint strength at ambient temperatures
d	diameter of brace	P_θ	ultimate joint strength at elevated temperatures
T	wall thickness of chord	β	ratio of brace diameter to chord diameter (=d/D)
t	wall thickness of brace	γ	ratio of chord diameter to twice chord thickness (=$D/2T$)
g	gap length between weld toes of braces	θ	brace-to-chord intersection angle

Currently, there is no design method to calculate the ultimate strength capacity of these joints at elevated temperatures. It may be possible to use the equations for ambient temperature design in design codes such as Eurocode EN 1993-1-8 [4] or design guide such as CIDECT guide No. 1 [16] and by replacing the yield stress of steel at ambient temperature by that at the elevated temperature. However, this approach may not be appropriate. These equations have been derived based on small deflections in the chord face. At elevated temperatures, as observed by Nguyen et al. [12], the chord face may undergo large distortions and their effects should be considered.

The purpose of this paper is to investigate the ultimate capacity of welded steel tubular joints at elevated temperatures, based on the results of finite element (FE) simulations of CHS or SHS tubular joints with axially loaded brace member at different elevated temperatures using the commercial Finite Element software ABAQUS v6.10-1. After validating the simulation model, extensive numerical simulations were conducted on T-, Y-, X-, N- and non-overlapped K-joints subjected to brace axial compression or tension, considering a wide range of geometrical parameters. The computed results were used to check whether it is appropriate to only modify the yield stress of steel for temperature effect for different joint types, geometric parameters and loading conditions.

2. Validation of finite element model

The general finite element package ABAQUS/Standard v6.10-1 [1] was used. For validation, the experimental results of Nguyen et al. [12] on tubular T-joints (Fig. 1a) at 20 °C, 550 °C and 700 °C, which appear to be the only ones to have been carried out for welded tubular joints at elevated temperatures, and the test results of Kurobane et al. [8] on K-joints (G2C-joint, Fig. 1b) at ambient temperature, were used. Owing to symmetry in loading and geometry, to reduce computational time, only a quarter of the T-joints and one half of the K-joints were modelled, with the boundary conditions for symmetry being applied to the nodes in the various planes of symmetry.

Table 1 summarises the geometric parameters of the T- and K-joints. The dimensionless parameter, β is the ratio of the brace diameter to the chord diameter (=d/D); and θ is the angle between the brace and chord members.

The elevated temperature tests of Nguyen et al. [12] were carried out under steady state in which the temperature of the structure was raised to the required level and the mechanical load was then applied. Because of this, the Riks method was chosen to simulate the large deformation behaviour.

2.1. Material properties

For the tubular T-joints tested by Nguyen et al. [12], the steel grade was S355 with a yield strength f_y = 380.3 N/mm^2 and an ultimate strength f_u = 519.1 N/mm^2 from the coupon tests at ambient temperature. The elastic modulus of steel was assumed to be 210 GPa. The elevated temperature stress–strain curves were based on Eurocode EN-1993-1-2 [3]. In the ABAQUS simulation model, the true stress–strain curve was input after converting the engineering stress–strain curve into the true stress and logarithmic strain curve by using the following equations [2]:

$$\varepsilon_T = \ln(1+\varepsilon) \tag{1}$$

$$\sigma_T = \sigma(1+\varepsilon) \tag{2}$$

where ε_T is the true strain, ε the engineering strain, σ_T the true stress and σ is the engineering stress.

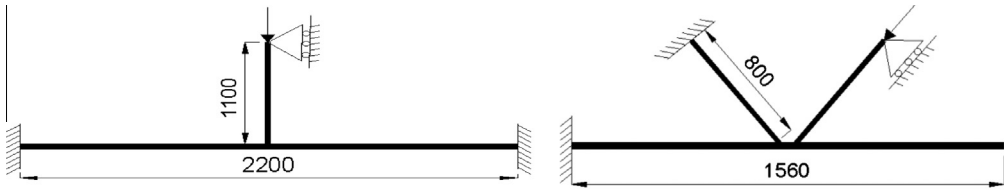

(a) PT3-joint (Nguyen et al., 2010a) (b) G2C- joint (Kurobane et al., 1986)

Fig. 1. Tested joints used for validation.

Table 1
Joint test specimens used for FE model validation.

Joint name	D (mm)	d (mm)	T (mm)	t (mm)	g (mm)	β (d/D)	θ (°)
PT3 (Nguyen et al. [12])	244.5 (L = 2200)	168.3 (l = 1100)	6.3	6.3	–	0.69	90
G2C [8]	216.4 (L = 1560)	165.0 (l = 800)	7.82	5.28	29.5	0.76	60

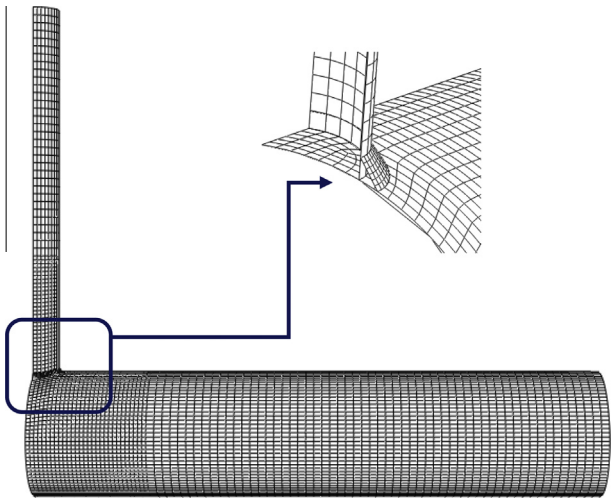

Fig. 2. Mesh layout.

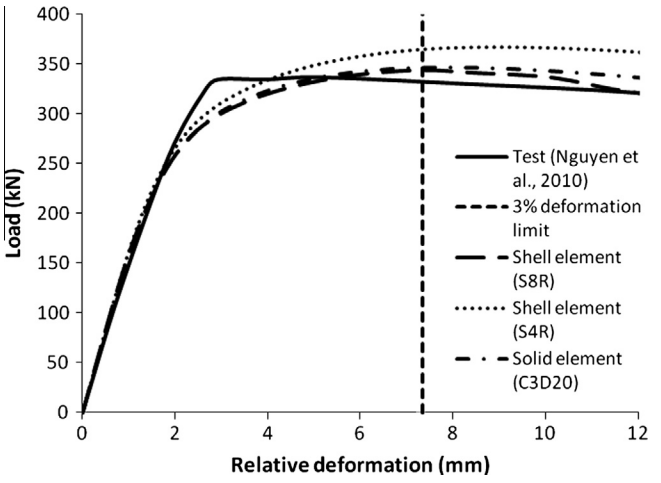

Fig. 4. Comparisons for using different element types at ambient temperature, test PT3 (Nguyen et al. [12]).

For the K-joint tests performed by Kurobane et al. [8], the nominal yield strengths were $f_{y,c} = 480$ N/mm^2, $f_{y,b} = 363$ N/mm^2 and the ultimate strengths were $f_{u,c} = 532$ N/mm^2, $f_{u,b} = 436$ N/mm^2 for the chord and brace members respectively.

In the numerical simulation model, the Von-Misses yield surface criterion and isotropic strain hardening rules were used.

2.2. Mesh convergence

A mesh convergence study was carried out to determine a suitable FE model for the analysis. The same mesh size was then applied to all models. ABAQUS element type S8R was used. Model PT3 of the tests by Nguyen et al. [12] was selected for this case. Fig. 2 shows the mesh layout. Fig. 3(a) and (b) presents the mesh sensitivity study results for the tubular sections and for the weld in the joint zone near the welds. Mesh sizes of 10 mm and 5 mm were suitable for the tubular members and the weld.

Outside the joint zone, a coarse mesh (20 mm) can be used.

2.3. Finite element type

For the chord and brace members, ABAQUS element types C3D20R (20 noded solid element), S8R (8-noded quadrilateral shell element) or S4R (four noded shell element) may be used. For weld modelling, quadratic wedge solid element (C3D15), eight noded thick shell element (S8R) or four noded shell element (S4R) may be used. At the weld-tubular section interface, the brace and chord members were tied with the weld elements using the ABAQUS "tie" function with surface to surface contact. The brace and chord members were chosen as the master surface and the weld elements were the slave surface.

Fig. 4 compares the simulation and test load–deflection curves of test PT3 of Nguyen et al. [12] at ambient temperature. Also shown in Fig. 4 is the 3% deflection limit ($0.03d_0$), according to Lu et al. [10] which is used to determine the ultimate load carrying capacity of the joints. From the comparisons, it can be seen that the eight-noded thick shell elements and solid elements give close prediction of the test result of Nguyen, but using the four-noded shell elements overestimate the ultimate capacity of PT3 joint. The tested joint had some initial plastic deformations due to faulty operation of the hydraulic jack during the loading step as reported by Nguyen et al. However, this did not affect the ultimate strength and post-peak behaviour, which were closely simulated by the numerical model.

Furthermore, Table 2 summarises the finite element results for using the different types of element. As already mentioned, using the four-noded shell elements (S4R) overestimated the joint load carrying capacity. Although both the eight-noded thick shell and solid elements gave good results, modelling the joint with solid elements required considerably more computational time than using the shell elements. In particular, when using solid elements, ABAQUS requires at least two layers of elements so as not to overestimate the real behaviour.

As a recommendation, eight-noded thick shell elements (S8R) with 5 integration points through the element thickness are suitable to model the brace and chord members. The same method

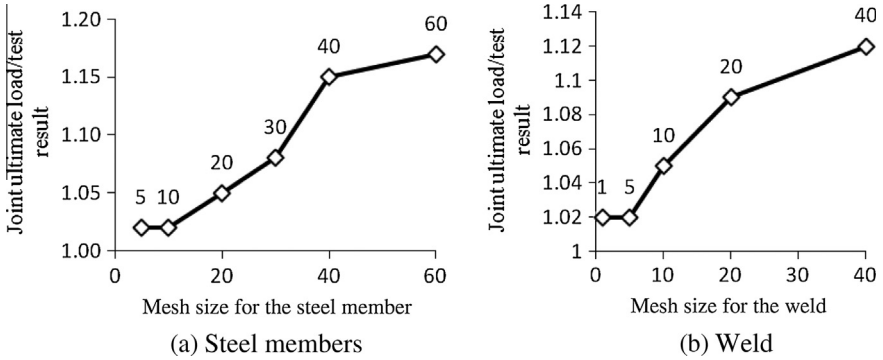

Fig. 3. Mesh sensitivity study results.

Table 2
Sensitivity of numerical results for test PT3 of Nguyen et al. [12] at ambient temperature.

	Number of elements	Relative CPU-time	Ultimate load (kN)	Strength ratio
Test results of Nguyen et al. [12]	–	–	338.8	1.00
Solid elements (C3D15)	9699	11.9	346.5	1.02
Shell elements (S8R)	3555	1.00	343.4	1.01
Shell elements (S4R)	3555	0.24	366.8	1.08

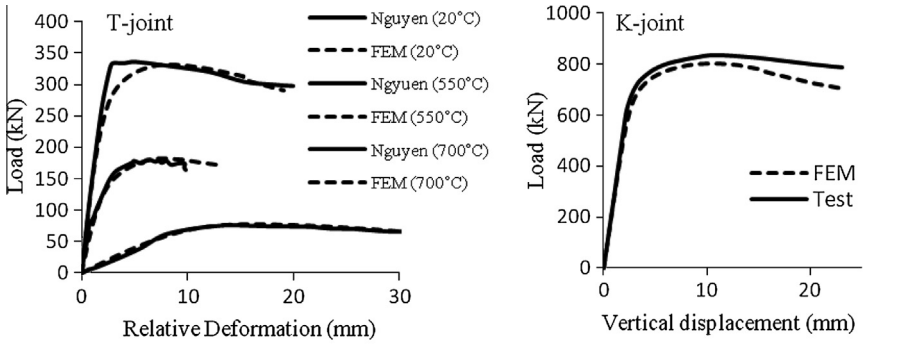

(a) PT3-joint (Nguyen et al., 2010a) (b) G2C- joint (Kurobane et al., 1986)

Fig. 5. Comparison for load–displacement curves for T- and K-joints.

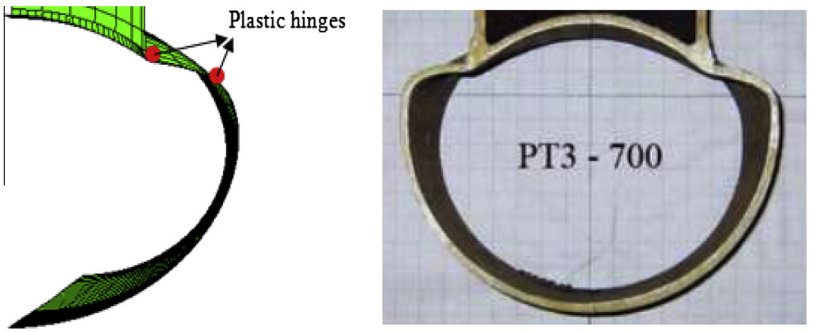

(a) Simulation (b) Test observation (Nguyen et al., 2010a)

Fig. 6. Deformed shapes of joint PT3 at 700 °C.

was used by Van der Vegte [15]. For modelling the weld, quadratic wedge solid elements (C3D15) can be used for accurate meshing of the weld geometry [6].

2.4. Validations against available test results

Fig. 5(a) compares the simulation load–deflection curves with the test results of Nguyen et al. [12] for joint PT3 at three different temperatures. The relative displacement refers to the difference of the axial displacement of the brace (δ) relative to the central chord. In all cases, the agreement is excellent for the T-joints. For the K-joint, the results in Fig. 5(b) also indicate very good agreement. Fig. 6 further compares the simulated and observed deformed shapes of PT3 joint at 700 °C. The numerical model was clearly a faithful representation of the test.

From these comparisons, it can be concluded that the numerical simulation model is suitable for simulating the behaviour of T- and K-welded tubular joints. These models were used to conduct the parametric study in the next section to obtain the ultimate load carrying capacities of welded tubular joints at different temperatures.

3. Parametric study

Fig. 7 shows the joint configurations investigated in the parametric study, including T-, Y-, X-, N- and non-overlapped K-joints subject to brace axial compression or tension.

Table 3 lists the geometrical parameters considered in the parametric study. Table 3 also illustrates the loading and boundary conditions. Details of the case studies and the reasons for selecting them are as follows:

(Case 1) T-joints were analysed under brace compression load in order to examine the effects of global bending of the chord member and large distortions (flattening) at the chord face on the ultimate strength of tubular joints at elevated temperatures. Table 4 lists the detailed parameters considered. The investigated parameters include the ratio of brace to chord diameter (β), the ratio of chord diameter to thickness (γ) and the tubular section type (CHS or SHS).
(Case 2) X-joints subject to brace axial compression or tension, considering different brace angles, were modelled to exclude the global bending effect. Table 5 shows the geometric parameters.

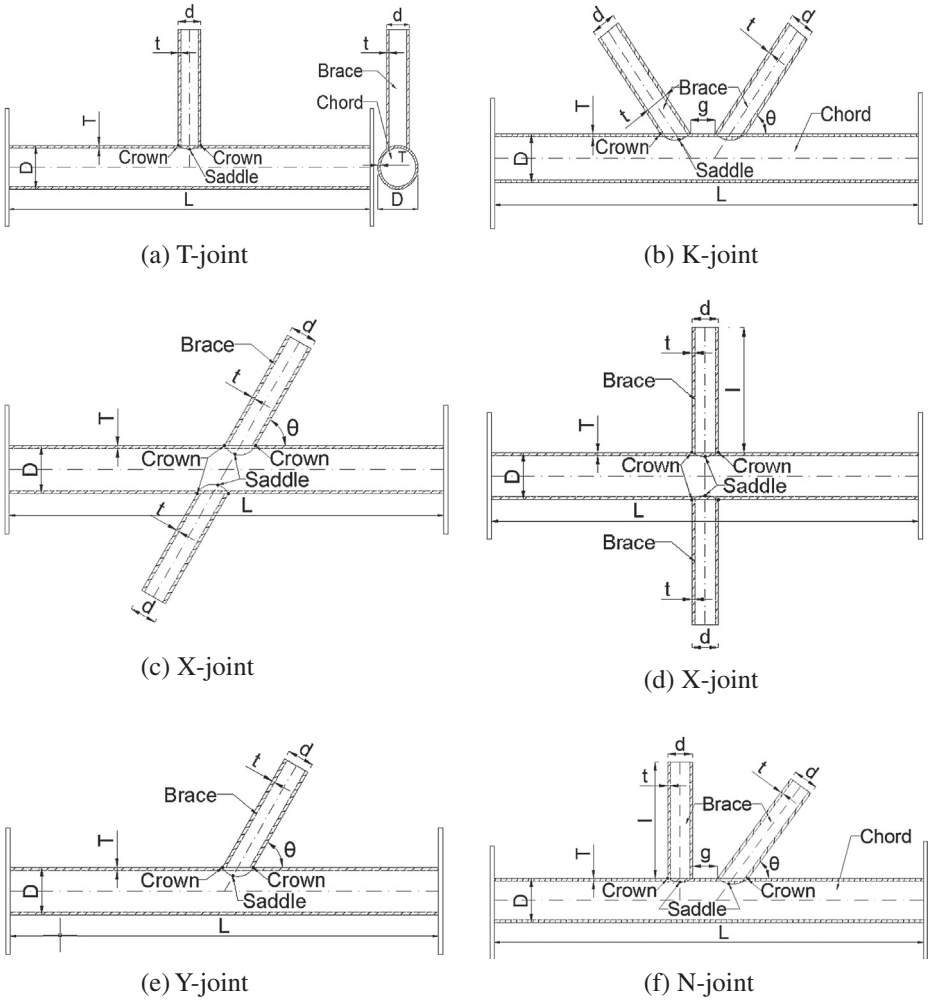

Fig. 7. Joint configurations used in the parametric study.

Table 3
Summary of simulation cases with load and boundary conditions.

Case studies	Parameters	Boundary and loading conditions
Case 1: T-joints – compressive brace member	• β, Ratio of brace diameter to chord diameter (=d/D) • Γ, Ratio of chord diameter to twice chord thickness (=$D/2T$) • Section type	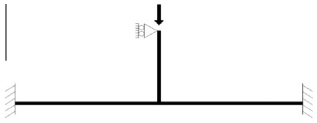
Case 2: X-joints	• θ, Brace-to-chord intersection angle • Brace loading directions	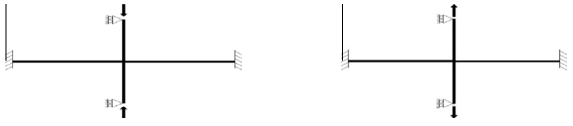
Case 3: T-joints – tensile brace member	• β, Ratio of brace diameter to chord diameter (=d/D) • Γ, Ratio of chord diameter to twice chord thickness (=$D/2T$) • Section type	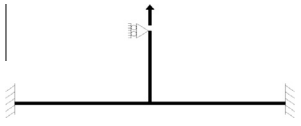
Case 4: K-joints and N-joints	• β, Ratio of brace diameter to chord diameter (=d/D) • θ, Brace-to-chord intersection angle	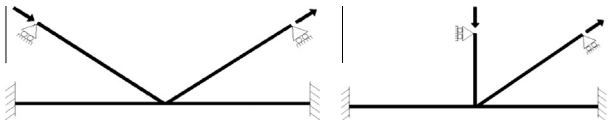
Case 5: Y-joints	• θ, Brace-to-chord intersection angle • Brace loading directions	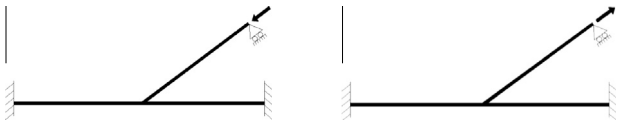

Table 4
Geometrical parameters for T-joints with compressive brace member (see Case 1 in Table 3).

Joint type	Joint name	D (mm)	d (mm)	T (mm)	t (mm)	γ ($D/2T$)	β (d/D)	θ (°)
CHS T-joints	CTC1	244.5 (L = 2200)	168.3 (l = 1000)	6.3	6.3	19.4	0.69	90
	CTC2	244.5 (L = 2200)	139.7 (l = 1000)	6.3	6.3	19.4	0.57	90
	CTC3	244.5 (L = 2200)	114.3 (l = 1000)	6.3	6.3	19.4	0.47	90
	CTC4	323.9 (L = 4000)	193.7 (l = 1000)	10	10	16.2	0.60	90
	CTC5	323.9 (L = 3000)	168.3 (l = 1000)	10	10	16.2	0.52	90
	CTC6	323.9 (L = 3000)	139.7 (l = 1000)	10	10	16.2	0.43	90
	CTC7	323.9 (L = 3000)	114.3 (l = 1000)	10	10	16.2	0.35	90
	CTC8	323.9 (L = 4000)	193.7 (l = 1100)	8	8	20.2	0.60	90
	CTC9	323.9 (L = 4000)	193.7 (l = 1100)	12.5	12.5	13.0	0.60	90
	CTC10	323.9 (L = 4000)	193.7 (l = 1100)	16	16	10.1	0.60	90
SHS T-joints	STC1	323.9 (L = 4000)	193.7 (l = 1100)	10	10	16.2	0.60	90
	STC2	300 (L = 4000)	200 (l = 1100)	10	10	15.0	0.67	90
	STC3	300 (L = 4000)	150 (l = 1100)	10	10	15.0	0.50	90
	STC4	300 (L = 4000)	120 (l = 1100)	10	10	15.0	0.40	90
							Total	162

Table 5
Geometrical parameters for X-joints (see Case 2 in Table 3).

Joint type	Joint name	D (mm)	d (mm)	T (mm)	t (mm)	β (d/D)	θ (°)
CHS X-joints	CXC1	323.9 (L = 4000)	193.7 (l = 1100)	10	10	0.60	90
	CXT1	323.9 (L = 4000)	193.7 (l = 1100)	10	10	0.60	90
	CXC2	323.9 (L = 4000)	193.7 (l = 1100)	10	10	0.60	45
	CXT2	323.9 (L = 4000)	193.7 (l = 1100)	10	10	0.60	45
	CXC3	323.9 (L = 4000)	193.7 (l = 1100)	10	10	0.60	60
	CXT3	323.9 (L = 4000)	193.7 (l = 1100)	10	10	0.60	60
SHS X-joints	SXC1	323.9 (L = 4000)	193.7 (l = 1100)	10	10	0.60	90
	SXT1	323.9 (L = 4000)	193.7 (l = 1100)	10	10	0.60	90
						Total	64

Table 6
Geometrical parameters for T-joints with tensile brace member (see Case 3 in Table 3).

Joint type	Joint name	D (mm)	d (mm)	T (mm)	t (mm)	γ ($D/2T$)	β (d/D)	θ (°)
CHS T-joints	CTT1	323.9 (L = 4000)	193.7 (l = 1100)	8	8	20.2	0.60	90
	CTT2	323.9 (L = 4000)	193.7 (l = 1100)	12.5	12.5	13.0	0.60	90
	CTT3	323.9 (L = 4000)	193.7 (l = 1100)	10	10	16.2	0.60	90
	CTT4	323.9 (L = 4000)	168.3 (l = 1100)	10	10	16.2	0.52	90
	CTT5	323.9 (L = 4000)	139.7 (l = 1100)	10	10	16.2	0.43	90
	CTT6	323.9 (L = 4000)	114.3 (l = 1100)	10	10	16.2	0.35	90
SHS T-joints	STT1	323.9 (L = 4000)	193.7 (l = 1100)	10	10	16.2	0.60	90
	STT2	300 (L = 4000)	200 (l = 1100)	10	10	15.0	0.67	90
	STT3	300 (L = 4000)	150 (l = 1100)	10	10	15.0	0.50	90
	STT4	300 (L = 4000)	120 (l = 1100)	10	10	15.0	0.40	90
							Total	80

Table 7
Geometrical parameters for K-joints (see Case 4 in Table 3).

Joint type	Joint name	D (mm)	d (mm)	T (mm)	t (mm)	g (mm)	β (d/D)	θ (°)
CHS K-joints	CK1	219.1 (L = 1500)	193.7 (l = 1100)	6.3	6.3	30	0.88	60
	CK2	219.1 (L = 1500)	168.3 (l = 1100)	6.3	6.3	30	0.77	60
	CK3	219.1 (L = 1500)	114.3 (l = 1100)	6.3	6.3	30	0.52	60
	CK4	323.9 (L = 4000)	193.7 (l = 1100)	10	10	30	0.60	30
SHS K-joint	SK1	300 (L = 4000)	150 (l = 1100)	10	10	30	0.5	60
							Total	40

(Case 3) This case is directly opposite to Case 1. Here the brace member in the T-joints was in tension. Table 6 lists the parameters considered.
(Case 4) Table 7 lists the parameters for the K-joints. For these joints, one brace member was in tension and the other in compression and the loads were equal to eliminate the effects of global bending and flattening of the chord. The brace angles were set at 60°. Furthermore, CHS N-joints (by setting one of the brace members of the K-joint perpendicular to the chord) were performed. Table 8 lists the geometrical parameters considered.

Table 8
Geometrical parameters for N-joints (see Case 4 in Table 3).

Joint type	Joint name	D (mm)	d (mm)	T (mm)	t (mm)	g (mm)	β (d/D)	θ (°)
CHS N-joints	CN1	323.9 (L = 4000)	193.7 (l = 1000)	10	10	30	0.6	45
	CN2	323.9 (L = 4000)	168.3 (l = 1000)	10	10	30	0.52	45
	CN3	323.9 (L = 4000)	139.7 (l = 1000)	10	10	30	0.43	45
							Total	24

Table 9
Geometrical parameters for Y-joints (see Case 5 in Table 3).

Joint type	Joint name	D (mm)	d (mm)	T (mm)	t (mm)	γ ($D/2T$)	β (d/D)	θ (°)
CHS Y-joints	CYC1	323.9 (L = 4000)	193.7 (l = 1000)	10	10	16.2	0.60	30
	CYC2	323.9 (L = 4000)	193.7 (l = 1000)	10	10	16.2	0.60	45
	CYC3	323.9 (L = 4000)	193.7 (l = 1000)	10	10	16.2	0.60	60
	CYC4	323.9 (L = 4000)	193.7 (l = 1000)	8	8	20.2	0.60	45
	CYC5	323.9 (L = 4000)	193.7 (l = 1000)	12.5	12.5	13.0	0.60	45
	CYC6	323.9 (L = 4000)	193.7 (l = 1000)	16	16	10.1	0.60	45
	CYT1	323.9 (L = 4000)	193.7 (l = 1000)	10	10	16.2	0.60	30
	CYT2	323.9 (L = 4000)	193.7 (l = 1000)	10	10	16.2	0.60	45
	CYT3	323.9 (L = 4000)	193.7 (l = 1000)	10	10	16.2	0.60	60
							Total	72

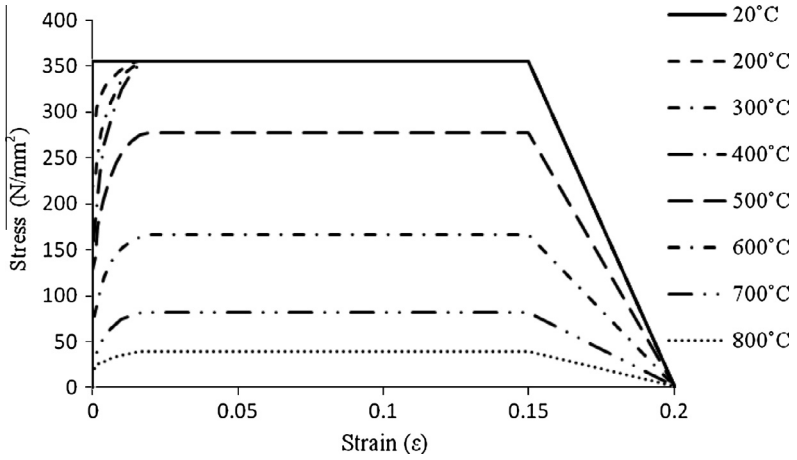

Fig. 8. Stress–strain relationships at elevated temperatures.

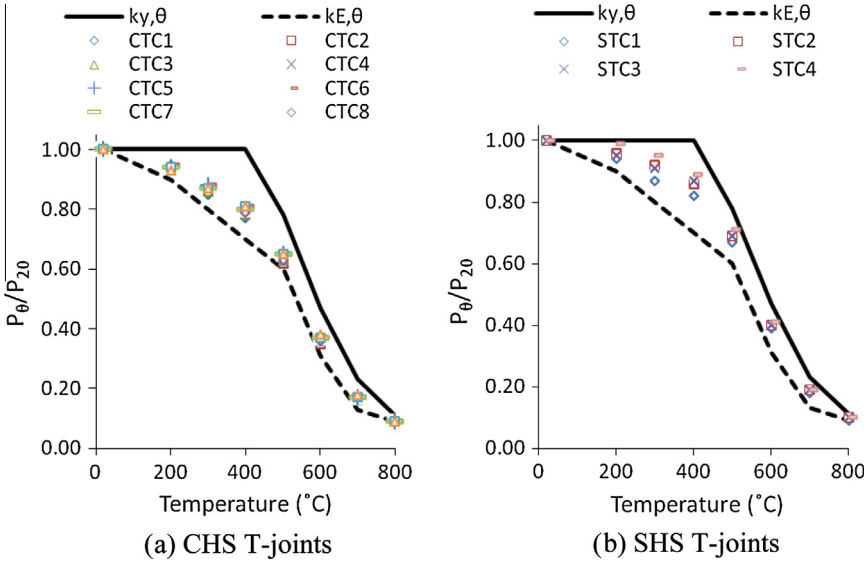

Fig. 9. Comparison for T-joints with compressive brace member.

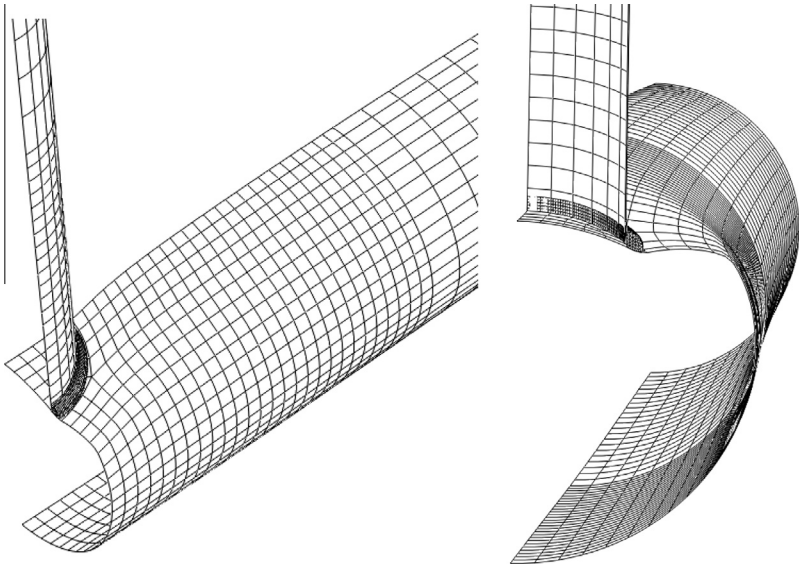

Fig. 10. Deformations of the CTC5 joint at 700 °C.

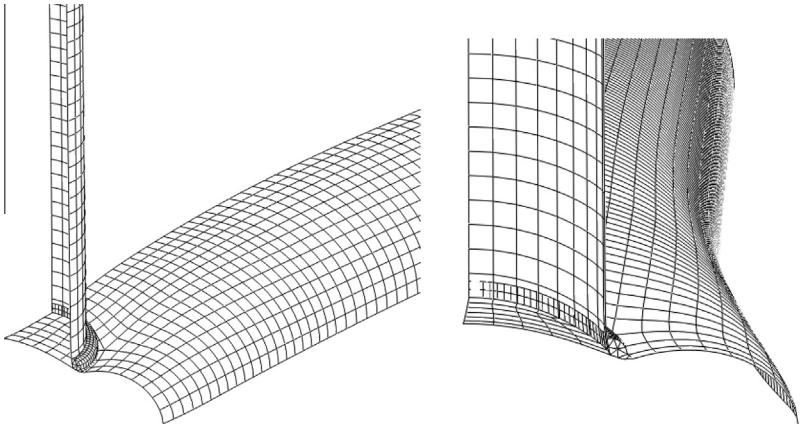

Fig. 11. Deformations of the CXC1 joint at 700 °C.

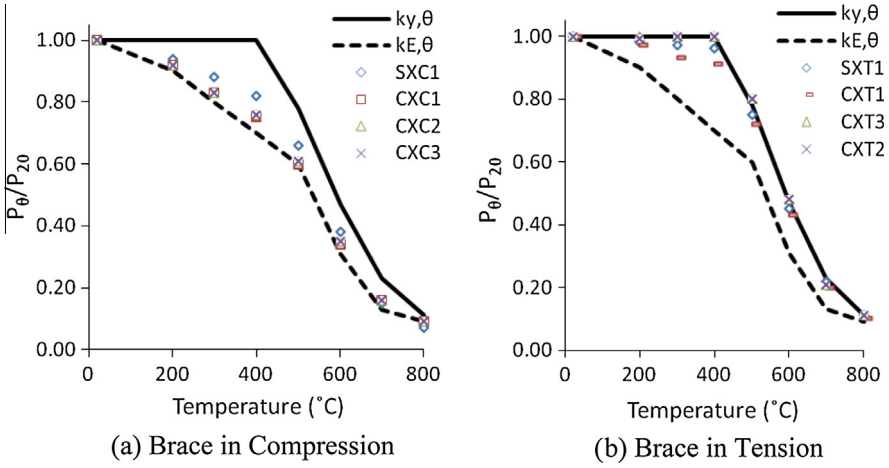

Fig. 12. Comparison for CHS and SHS X-joints with the brace members in equal compression or tension.

(Case 5) Changing the angle of the brace member to the chord member from 90° in the T-joint to different values makes Y-joint. Different values of this angle (θ = 30°, 45° and 60°) were simulated to investigate its effect.

Table 9 lists the geometrical parameters for the Y-joints.

For identification, the name of each joint consists of three letters, the first one (C or S) representing the tubular cross-section shape (CHS or SHS), the second indicating joint type, and the third

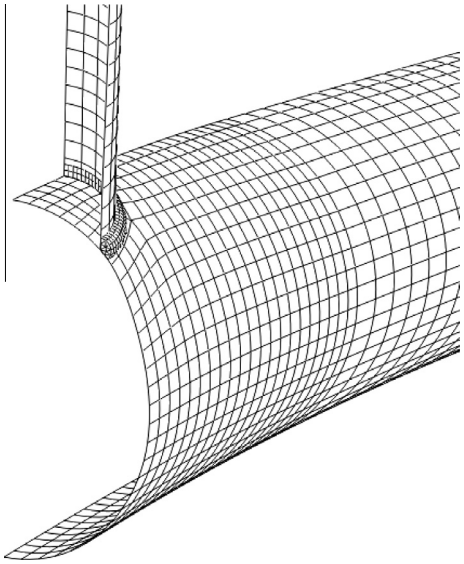

Fig. 13. Deformations of the CTT5 joint at 700 °C.

giving the brace loading direction (Tension or Compression). For example, CTC1 means CHS – T-joint with the brace member subjected to an axial compression load.

To obtain the joint resistance values, steady state analysis was used. In this case, the effect of temperature was to change the mechanical properties of the steel. However, the results are applicable to the transient condition as demonstrated by the comparison between the steady state and transient state analysis results in Section 3.3.

3.1. Material properties and boundary conditions

In the numerical analyses, the elevated engineering temperature stress–strain curves of the steel were based on Eurocode EN-1993-1-2 as shown in Fig. 8 [3]. The yield stress and modulus of elasticity at ambient temperature were 355 N/mm^2 and 210 GPa respectively and the Poisson's ratio was 0.3. Uniform temperature distribution was assumed throughout the joint. Furthermore, the Von-Misses yield surface criterion and isotropic strain hardening rules were used in order to represent the yielding of steel.

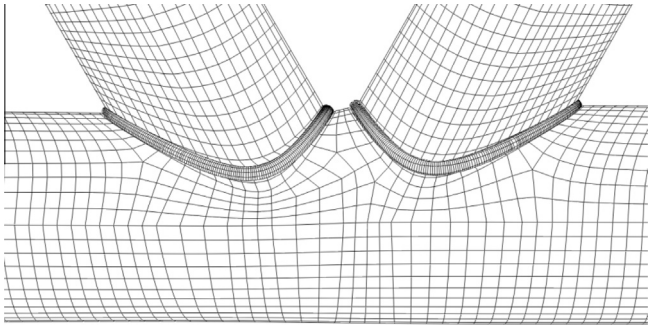

Fig. 15. Deformations of the CK1 joint at 700 °C.

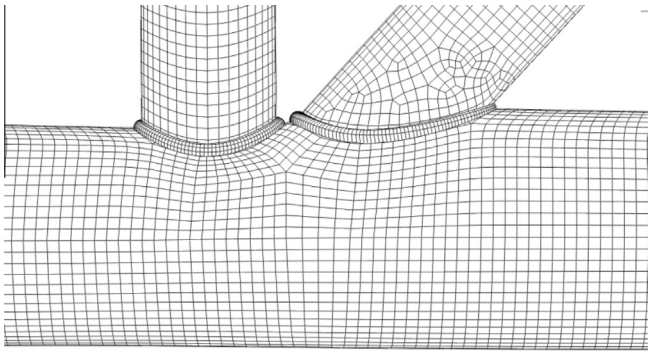

Fig. 16. Deformations of the CN3 joint at 700 °C.

3.2. Simulation results and discussion

In the results to be presented, the joint strength ratio (P_θ/P_{20}) is used, being the ratio of the joint strength at elevated temperature θ to that at ambient temperature. The joint strength ratios at different temperatures are compared to the steel strength and modulus of elasticity reduction factors at elevated temperatures. Appendix A presents the load ratios for each joint, based on the numerical results.

3.2.1. Case 1: T-joints with brace member in compression

The results are divided into two groups. The first group focuses on the effects of changing β and γ values on the joint strength ratio

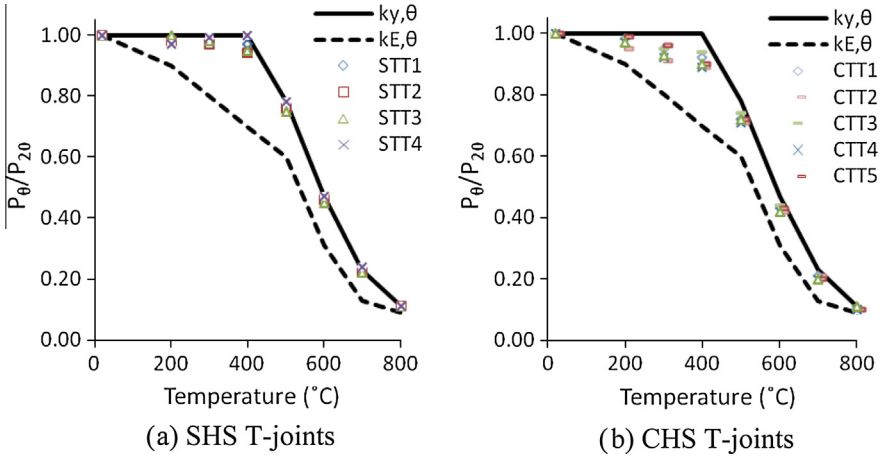

Fig. 14. Comparisons for T-joints with the brace member in tension.

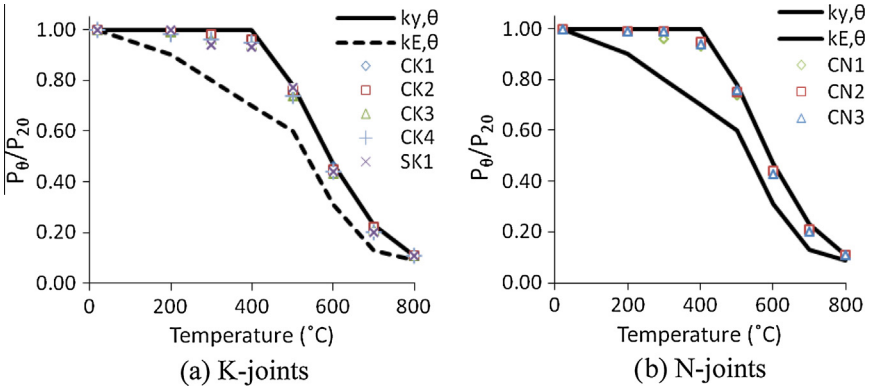

Fig. 17. Comparison for K- and N-joints.

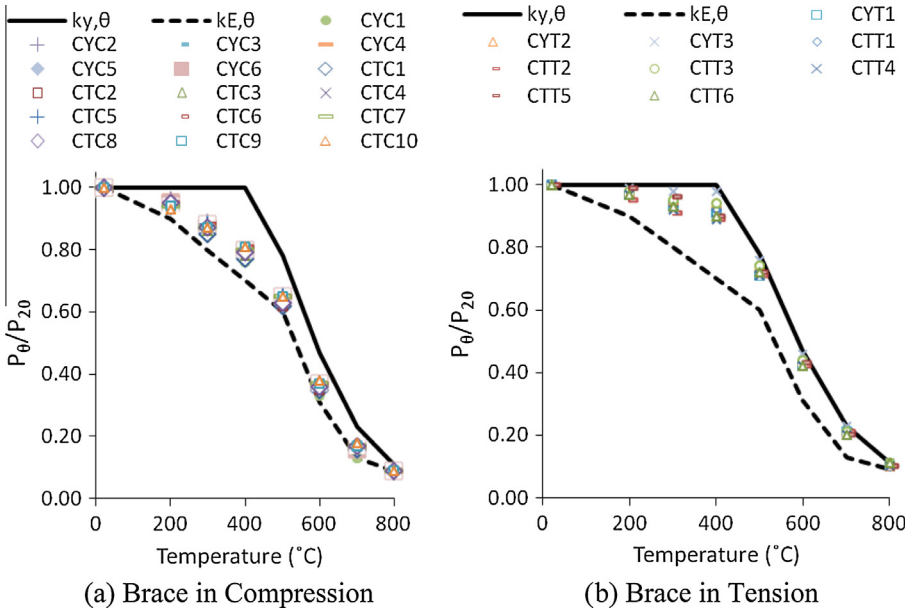

Fig. 18. Comparison for CHS Y- and T-joints with the brace member in compression or tension.

Table 10
Comparison of steady state and transient state failure temperatures for CTC4 and CK3 joints.

	Transient failure temperatures (in brackets) at loads (kN) equal to steady state resistances at different temperatures						
Steady state temperature	20 °C	200 °C	300 °C	400 °C	500 °C	600 °C	700 °C
CTC4	561.1 (20 °C)	533.1 (199 °C)	488.2 (297 °C)	448.9 (398 °C)	359.1 (496 °C)	202.0 (595 °C)	95.4 (695 °C)
CK3	301.1 (20 °C)	298.1 (201 °C)	289.1 (302 °C)	283.0 (404 °C)	222.8 (496 °C)	129.5 (598 °C)	63.2 (698 °C)

Table 11
FE results for CHS T-joints.

Temperature (°C)	CHS									
	CTC1	CTC2	CTC3	CTC4	CTC5	CTC6	CTC7	CTC8	CTC9	CTC10
20	1.00	1.00	1.00	1.00	1.00	1.00	1.00	1.00	1.00	1.00
200	0.94	0.94	0.93	0.95	0.94	0.95	0.94	0.95	0.94	0.93
300	0.85	0.87	0.86	0.87	0.88	0.88	0.87	0.87	0.87	0.87
400	0.77	0.79	0.78	0.80	0.80	0.81	0.80	0.79	0.81	0.81
500	0.62	0.62	0.63	0.64	0.65	0.65	0.65	0.63	0.65	0.65
600	0.35	0.35	0.36	0.36	0.37	0.37	0.37	0.36	0.37	0.38
700	0.16	0.16	0.16	0.17	0.17	0.17	0.17	0.17	0.17	0.18
800	0.09	0.09	0.09	0.09	0.09	0.09	0.09	0.09	0.09	0.09

Table 12
FE results for SHS T-joints.

Temperature (°C)	SHS				EN 1993-1-2	
	STC1	STC2	STC3	STC4	ky, θ	kE, θ
20	1.00	1.00	1.00	1.00	1.00	1.00
200	0.94	0.96	0.95	0.99	1.00	0.90
300	0.87	0.92	0.91	0.95	1.00	0.80
400	0.82	0.86	0.87	0.89	1.00	0.70
500	0.67	0.69	0.69	0.71	0.78	0.60
600	0.39	0.40	0.40	0.41	0.47	0.31
700	0.18	0.19	0.19	0.19	0.23	0.13
800	0.09	0.10	0.10	0.10	0.11	0.09

Table 14
FE results for SHS T-joint under tension load.

Temperature (°C)	SHS				EN 1993-1-2	
	STT1	STT2	STT3	STT4	ky, θ	kE, θ
20	1.00	1.00	1.00	1.00	1.00	1.00
200	0.98	0.98	1.00	0.97	1.00	0.90
300	0.97	0.97	0.98	0.99	1.00	0.80
400	0.97	0.94	0.95	1.00	1.00	0.70
500	0.76	0.76	0.75	0.78	0.78	0.60
600	0.45	0.46	0.45	0.47	0.47	0.31
700	0.22	0.22	0.22	0.24	0.23	0.13
800	0.11	0.11	0.11	0.11	0.11	0.09

of (CHS) T-joints. The second group compares the effect of tubular section type (CHS or SHS).

Fig. 9 compares the strength ratios with the steel yield strength and modulus of elasticity reduction factors at elevated temperatures. It can be seen that for both CHS and SHS T-joints, the numerical simulation strength ratios are generally lower than the reduction factors for the yield strength of steel at elevated temperatures. The joint strength reduction for SHS joints is higher than for CHS joints.

Two factors contribute to the higher reduction in joint strength than the reduction in steel yield stress at elevated temperatures. Fig. 10 shows the deformed shape of a quarter of CTC5 joint at 700 °C. When a T-joint is under brace compression load, the connected chord wall is in compression from global bending of the chord. This compression force in the chord member produces some additional local bending moment when the chord compression acts on the deformation of the chord face (local P–δ effect). At the same time, the side faces of the chord member experience local bulging (ovalisation) under the brace compression, causing the chord side wall to flatten. Both effects prevent the joint from reaching the yield line capacity of the chord face which is based on the original undeformed chord face.

At elevated temperatures, both effects increase due to increased deformations as a result of reduced steel stiffness. Therefore, the joint failure loads decrease faster than the steel yield strength at elevated temperatures as shown in Fig. 9(a) and (b). Furthermore, the strength reductions at elevated temperatures are greater for CHS joints than for SHS joints because the extent of flattening is much greater in the CHS chord member than in the SHS chord member.

Detailed examination of the simulation results (Fig. 9a) reveals that changing the brace to chord dimension ratio β (=d/D) or the wall thickness ratio γ has little influence on the elevated temperature effects on joint strength, which is in agreement with the findings of Tan et al. [14].

These findings suggest that for both (CHS) and (SHS) T-joints under brace compression load, merely changing the ambient temperature yield strength of the steel to that at elevated temperature overestimates the ultimate load carrying capacity of the joint. Since the joint strength reduction is caused by deformation of the chord member, the joint strength reduction should be related to the deformation characteristics of the joint. Based on the above observation that the joint strength reduction is not influenced by the joint geometry and that using the reduction factor for the Young's modulus of steel at elevated temperature gives a close lower bound approximation to the joint strength reduction, it is suggested that for T-joints with the brace member in compression, the joint strength equation is modified by the Young's modulus reduction factor for steel at elevated temperatures.

3.2.2. Case 2: X-joints with the brace members in equal compression or tension

When an X-joint is subject to equal load in the two brace members, there is no global bending in the chord member. Fig. 11 shows the deformed shape of an eight of the complete CXC1 joint at 700 °C. Therefore, the above mentioned P-δ effect is eliminated. When the brace members are in tension, the local flattening of the chord member disappears. Therefore, it is expected that the yield-line equation for calculating the chord face capacity still applies provided the elevated temperature yield stress of the steel is used. The results in Fig. 12(b) confirm this expectation. However, when the brace members are in compression, the local flattening of the chord member still exists. The results in Fig. 12(a) suggest that the effect of local flattening is severe. Although the brace–chord angle has some influence, all the simulation results are close and just above the reduction factor for the Young's modulus of steel at elevated temperatures.

3.2.3. Case 3: T-joints with the brace member in tension

When the brace member of a T-joint is in tension, global bending of the chord member induces tension in the connected chord face. Therefore, the local P-δ effect disappears around the brace-to-chord intersection area. Also there is no longer any flattened of the chord face at the loaded region beneath the brace. This is shown in Fig. 13. Therefore, it is expected that the join strength can be calculated using the ambient temperature equation based on yield-line solution, but modified by the steel yield strength reduction factors at elevated temperatures. The results in

Table 13
FE results for X-joints.

Temperature (°C)	SHS		CHS						EN 1993-1-2	
	SXC1	SXT1	CXC1	CXT1	CXC2	CXT2	CXC3	CXT3	ky, θ	kE, θ
20	1.00	1.00	1.00	1.00	1.00	1.00	1.00	1.00	1.00	1.00
200	0.94	0.98	0.92	0.97	0.92	0.99	0.92	1.00	1.00	0.90
300	0.88	0.97	0.83	0.93	0.83	1.00	0.83	1.00	1.00	0.80
400	0.82	0.96	0.75	0.91	0.76	1.00	0.76	1.00	1.00	0.70
500	0.66	0.75	0.60	0.72	0.61	0.80	0.61	0.80	0.78	0.60
600	0.38	0.45	0.34	0.43	0.35	0.48	0.35	0.48	0.47	0.31
700	0.15	0.22	0.16	0.20	0.16	0.21	0.16	0.21	0.23	0.13
800	0.07	0.11	0.09	0.10	0.09	0.11	0.09	0.11	0.11	0.09

Table 15
FE results for CHS T-joint under tensile load.

Temperature (°C)	CHS						EN 1993-1-2	
	CTT1	CTT2	CTT3	CTT4	CTT5	CTT6	ky, θ	kE, θ
20	1.00	1.00	1.00	1.00	1.00	1.00	1.00	1.00
200	0.98	0.95	0.98	0.97	0.99	0.97	1.00	0.90
300	0.95	0.91	0.95	0.92	0.96	0.93	1.00	0.80
400	0.92	0.89	0.94	0.89	0.90	0.90	1.00	0.70
500	0.72	0.71	0.74	0.71	0.72	0.72	0.78	0.60
600	0.43	0.42	0.44	0.42	0.43	0.42	0.47	0.31
700	0.21	0.21	0.21	0.20	0.20	0.20	0.23	0.13
800	0.10	0.10	0.11	0.10	0.10	0.11	0.11	0.09

Fig. 14(a) and (b) for both SHS and CHS joints confirm this. This effect is slightly higher for joints with smaller brace to chord dimension ratios (β). Nevertheless, this effect is relatively small and it is acceptable to use the yield strength reduction factor for the joint strength reduction at elevated temperatures.

3.2.4. Case 4: K-joints and N-joints with equal but opposite loads in the brace members

The brace members in a K-joint usually have equal, but opposite, forces. This eliminates global bending as well as local flattening in the chord member as shown in Fig. 15. The results in Fig. 17(a) show that in this case, the joint strength can be calculated using the ambient temperature equation and the elevated temperature yield strength of steel.

Due to the different directions of the brace forces, there was some axial force in the chord member. CK4 joint, which had a long chord length and small brace-to-chord intersection angle ($\theta = 30°$, $\beta = 0.60$ and $L = 4000$), was selected to investigate the influence of the horizontal components (along the chord members) of the brace forces on the ultimate load carrying capacity of the tubular joints at elevated temperatures. The brace forces would cause the highest tensile stresses in the left chord member and the greatest compressive stresses in the right chord member. Owing to the small magnitude of the brace forces compared to the compressive resistance of the chord members, the failure mode of CK4 was identical to other joints, being local plastification, rather than buckling, of the chord member. The joint failure loads were according to the effective yield strength reduction factors at elevated temperatures as shown in Fig. 17(a).

The behaviour of the N-joints (Fig. 17b) is consistent with the K-joints (Fig. 17a) because the global bending and local flattening effects are largely eliminated (Fig. 16) even though the two brace member loads do not produce exactly opposite effects.

3.2.5. Case 5: Y-joints

A Y-joint is similar to a T-joint except that the brace member is not perpendicular to the chord member. Therefore, it is expected that elevated temperatures have the same effect on the joint strength. This is confirmed by the results shown in Fig. 18(a) and (b) for Y-joints with the brace member in compression and tension respectively. Also, these figures include the relevant results for the T-joints.

3.3. Comparison between steady state and transient state analyses

The previous results were obtained from steady state analyses, in which the steel temperatures were increased to the desired level and followed by structural analysis at the elevated temperature. This was done because the analysis directly outputs the joint resistance. In realistic structures, the process is transient in which the load is applied first and then maintained when the temperature is increased. It is necessary to ensure that the steady state results are applicable to the transient condition.

CTC4 and CK3 joints were used as examples to investigate the differences between steady state and transient state analyses. The mechanical loads were applied at ambient temperature, the values being the same as their failure loads from the steady state analysis at the different temperature levels. The transient state analyses were then carried out to find the joint failure temperatures under the different loads.

Table 16
FE results for K-joints.

Temperature (°C)	K-joints					EN 1993-1-2	
	CK1	CK2	CK3	CK4	SK1	ky, θ	kE, θ
20	1.00	1.00	1.00	1.00	1.00	1.00	1.00
200	0.99	0.99	0.99	0.98	1.00	1.00	0.90
300	0.97	0.98	0.96	0.96	0.94	1.00	0.80
400	0.96	0.96	0.94	0.95	0.93	1.00	0.70
500	0.76	0.76	0.74	0.74	0.77	0.78	0.60
600	0.46	0.45	0.43	0.44	0.44	0.47	0.31
700	0.22	0.22	0.21	0.20	0.20	0.23	0.13
800	0.11	0.11	0.11	0.11	0.11	0.11	0.09

Table 17
FE results for N-joints.

Temperature (°C)	CHS N-joints			EN 1993-1-2	
	CN1	CN2	CN3	ky, θ	kE, θ
20	1.00	1.00	1.00	1.00	1.00
200	0.99	0.99	0.99	1.00	0.90
300	0.96	0.99	0.99	1.00	0.80
400	0.93	0.95	0.94	1.00	0.70
500	0.74	0.75	0.76	0.78	0.60
600	0.43	0.44	0.43	0.47	0.31
700	0.21	0.21	0.20	0.23	0.13
800	0.11	0.11	0.11	0.11	0.09

Table 18
FE results for Y-joints under compression.

Temperature (°C)	Under compression					
	CYC1	CYC2	CYC3	CYC4	CYC5	CYC6
20	1.00	1.00	1.00	1.00	1.00	1.00
200	0.96	0.96	0.95	0.97	0.95	0.95
300	0.88	0.89	0.89	0.89	0.88	0.88
400	0.76	0.80	0.81	0.80	0.80	0.80
500	0.62	0.65	0.65	0.65	0.65	0.65
600	0.33	0.37	0.37	0.37	0.36	0.37
700	0.13	0.16	0.17	0.16	0.16	0.16
800	0.09	0.09	0.09	0.09	0.09	0.09

Table 19
FE results for Y-joints under tension.

Temperature (°C)	Under tension			EN 1993-1-2	
	CYT1	CYT2	CYT3	ky, θ	kE, θ
20	1.00	1.00	1.00	1.00	1.00
200	0.97	0.98	0.99	1.00	0.90
300	0.93	0.95	0.98	1.00	0.80
400	0.91	0.94	0.98	1.00	0.70
500	0.71	0.74	0.76	0.78	0.60
600	0.42	0.44	0.46	0.47	0.31
700	0.21	0.21	0.23	0.23	0.13
800	0.10	0.10	0.11	0.11	0.09

Table 10 compares the steady state and transient state joint failure temperatures for the two example joints. The two sets of failure temperatures are very close, the maximum difference being 5 °C. This confirms that the steady state results are applicable to the transient state condition.

4. Conclusions

The main purpose of the paper has been to present the results of a numerical parametric study to investigate the effects of elevated temperatures on the ultimate load carrying capacity of welded steel tubular joints. Both CHS and SHS sections were considered. The joints investigated include T- and Y-joints with the brace member in tension or compression, X-joints with the two brace members in equal tension or equal compression and K- and N-joints with the two brace members with exactly opposite loads. The parametric study covered a range of different joint geometries for these different joint types. The elevated temperature mechanical properties of steel were based on Eurocode EN-1993-1-2 [3]. The main effect of elevated temperatures on joint strength is chord face flattening. Steady state analysis was used, but it has been shown that the results can be applied to the transient state.

Based on comparisons between the joint strength reduction factor with the steel yield stress and Young's modulus reduction factors at elevated temperatures, the following proposals are recommended for calculating joint strengths at elevated temperatures:

(1) For T-, Y- and X-joints with the brace member(s) in tension, and for K- and N-joints with the brace members under opposite loads, the joint strength reduction follows the steel yield strength reduction at elevated temperatures. Therefore, the existing CIDECT [16] or Eurocode EN 1993-1-8 [4] equations for ambient temperature design can be used, provided the steel yield strength at ambient temperature is replaced by that at the elevated temperature.
(2) For T-, Y- and X-joints with the brace member(s) in compression, it is not safe to use the above proposal. However, it is safe to use the joint strength calculation equations developed at ambient temperature, but the joint strength should be modified by the steel Young's modulus reduction factor at the elevated temperature.

Appendix A. Load ratios for tubular joints

A.1. Case 1: T-joints with brace member in compression

See Tables 11 and 12.

A.2. Case 2: X-joints with the brace members in equal compression or tension

See Table 13.

A.3. Case 3: T-joints with the brace member in tension

See Tables 14 and 15.

A.4. Case 4: K-joints and N-joints with equal but opposite loads in the brace members

See Tables 16 and 17.

A.5. Case 5: Y-joints

See Tables 18 and 19.

References

[1] Abaqus/Standard. Version 6.10-1. USA: K. a. S. Hibbit; 2011.
[2] Boresi AP, Schmidt RJ. Advanced mechanics of materials. 6th ed. John Wiley and Sons; 2003.
[3] CEN. Design of steel structures. Part: EN 1993-1-2-structural fire design. London: British Standard Institute; 2005.
[4] CEN. Design of Steel Structures. Part: EN 1993-1-8-design of joints. London: British Standard Institute; 2005.
[5] Cheng C, Yongbo S, Jie Y. Experimental and numerical study on fire resistance of circular tubular T-joints. J Constr Steel Res 2013;85:24–39.
[6] Cofer WF, Jubran JS. Analysis of welded tubular connections using continuum damage mechanics. J Struct Eng 1992;118(3):828–45.
[7] He S-B, Shao Y-B, Zhang H-Y, Yang D-P, Long F-L. Experimental study on circular hollow section (CHS) tubular K-joints at elevated temperature. Eng Fail Anal 2013;34:204–16.
[8] Kurobane Y, Ogawa K, Ochi K, Makino Y. Local buckling of braces in tubular K-joints. Thin-Wall Struct 1986;4(1):23–40.
[9] Liu ML, Zhao JC, Jin M. An experimental study of the mechanical behavior of steel planar tubular trusses in a fire. J Constr Steel Res 2010;66(4):504–11.
[10] Lu LH, De Winkel GD, Yu Y, Wardenier J. Deformation limit for the ultimate strength of hollow section joints. In: Proceedings of the sixth international symposium on tubular structures, Melbourne, Australia; 1994.
[11] Meng J, Jincheng Z, Minglu L, Jing C. Parametric analysis of mechanical behaviour of steel planar tubular truss under fire. J Constr Steel Res 2010;67(2011):75–83.
[12] Nguyen MP, Fung TC, Tan KH. An experimental study of structural behaviours of CHS T-joints subjected to brace axial compression in fire condition. In: Young, editor. Tubular structures XIII, CRC Press/Balkema; 2010.
[13] Nguyen MP, Tan KH, Fung TC. Numerical models and parametric study on ultimate strength of CHS T-joints subjected to brace axial compression under fire condition. In: Young, editor. Tubular structures XIII. The University of Hong Kong; 2010.
[14] Tan KH, Fung TC, Nguyen MP. Structural behaviour of CHS T-joints subjected to brace axial compression in fire condition. J Struct Eng 2012.
[15] Van der Vegte GJ. The static strength of uniplanar and multiplanar tubular T- and X-joints. Doctoral dissertation, Delft University of Technology; 1995.
[16] CIDECT. Design guide for circular hollow section (CHS) joints under predominantly static loading, Verlag TUV Rheinland, Germany; 2010.
[17] Yeoh S-K, Soh A-K, Soh C-K. Behaviour of tubular T-joints subjected to combined loadings. J Constr Steel Res 1995;32:259–80.
[18] Makino Y, Kurobane YKO, Van der Vegte GJ, Wilmshurst ST. Introduction to unstiffened CHS tubular joint database. In: Tubular Structure VII, Netherlands: Rotterdam; 1996. p. 157–164.
[19] Dexter E, Lee M. Static strength of axially loaded tubular K-joints. I: behavior. J Struct Eng 1999;125(2):194–201.
[20] Dexter E, Lee M. Static strength of axially loaded tubular K-joints. II: Ultimate capacity. J Struct Eng 1999;125(2):202–10.
[21] Lesani M, Bahaari MR, Shokrieh MM. Detail investigation on un-stiffened T/Y tubular joints behavior under axial compressive loads. J Constr Steel Res 2013;80:91–9.